Energy Conversion and Management 105 (2015) 488–497

Contents lists available at ScienceDirect

Energy Conversion and Management

journal homepage: www.elsevier.com/locate/enconman

Experimental study of redesigned draft tube of an Agnew microhydro turbine

Ammar Mirzaei [a,*], Mohammad Hassan Shojaeefard [b], Ali Babaei [b], Yousef Yassi [c]

[a] R&D Department, MAPNA Group Co., Tehran, Iran
[b] School of Mechanical Engineering, Iran University of Science and Technology, Tehran, Iran
[c] Iranian Research Organization for Science and Technology (IROST), Tehran, Iran

ARTICLE INFO

Article history:
Received 29 January 2015
Accepted 2 August 2015

Keywords:
Microhydro turbine
Surrogate-based optimization
Pressure recovery factor
Energy loss coefficient
Swirling flow

ABSTRACT

In this study, a surrogate-based optimization has been carried out for the components of an Agnew microhydro turbine. A neural network was constructed as the surrogate, while the Non-dominated Sorting Genetic Algorithm (NSGA-II) was used as the optimizer. The optimal design was found by numerical simulations, and the final design was manufactured and installed at the turbine outlet. The performance of the turbine components was then measured according to ASME performance test code. Comparison was carried out between the original draft tube and its modified under different operating conditions. The test results have confirmed that the pressure recovery factor of the new component increases by 20.3% and the loss coefficient diminishes by 4.0%, with regard to the original design under the best operating conditions.

1. Introduction

An Agnew turbine is a 45° inclined axial microhydro turbine whose blades can be adjusted to different angles. This type of turbine has been manufactured in different diameters (200, 300 and 500 mm) and installed at different sites in Scotland [1]. A scaled unit with a 150 mm tip diameter was manufactured at the Hydraulic Machines Laboratory (HML) of the Iranian Research Organization for Science and Technology (IROST) to investigate the applicability of the turbine for microhydro potentials in Iran [2].

Yassi [1] and Yassi et. al. [2] are the only researchers who has studied Agnew turbines, in which improvement of the turbine performance is investigated experimentally in design and part-load conditions. It is reported that installing guide vane mechanism improves the efficiency of the turbine as much as 23%, respected to the original design [2].

The draft tube in Agnew turbines is a diffuser, which connects the turbine outlet to the tailrace in order to recover the wasted kinetic energy at the runner outlet and convert it to a head rise and thus to increase the overall turbine efficiency. Since the Agnew turbine is a low-head axial type turbine operating at high rotation speeds, the performance of the draft tube has an important effect on turbine efficiency. The original draft tube of the turbine installed at the HML has been designed by simple traditional methods and by limiting the cone angle and the draft tube length.

The majority of literatures on this topic deal with the numerical investigation and experimental validation of flow phenomena occurring over the operating ranges of draft tubes and other components. In the last decade, the optimization of hydraulic turbine components has become more attractive to the researchers [3]. Lipej [4] used the Genetic Algorithm (GA) to perform a multi-objective geometry optimization of an axial flow hydro-turbine runner for various operating regimes. He found a region of low flow velocity behind the hub, in both the numerical and experimental approaches, which was minimized for the optimal design in order to reduce the energy loss in the draft tube. The optimal blade shape was determined by considering the chord-pitch ratio, the maximum profile thickness and the chamber position as the geometrical parameters, and the meridional velocity and the outlet vortex coefficient as the performance parameters. The efficiency of the final design was improved by 0.5% in the overload condition ($Q/Q_{opt} = 1.61$) and by up to 1.7% in the case of $Q/Q_{opt} = 0.39$.

Wu et al. [5] applied a CFD-based design optimization approach, in which the viscous 3D Navier-Stokes equations were solved by the STAR-CD in conjunction with the $k-\varepsilon$ turbulence model, to optimize the shape of the runner in a Francis turbine and its spiral casing. Comparison of the measured efficiencies of the old turbine

* Corresponding author.
E-mail address: mirzaei_a@mapnagroup.com (A. Mirzaei).

http://dx.doi.org/10.1016/j.enconman.2015.08.007
0196-8904/

Nomenclature

A	the area perpendicular to flow direction
AR	area ratio
ANN	artificial neural network
BC	boundary condition
ELC	energy loss coefficient
H	height above the tailrace
HML	hydraulic Machine Laboratory
I	turbulence intensity
K_u	circumferential blade speed ratio ($K_u = \frac{v}{\sqrt{2gL}}$)
L	head
M	modified case
N	rotational speed of turbine
n	normal vector of the surface
O	original case
P	pressure
PRF	pressure recovery factor
Q	flow rate
R	dynamometer unloading
RMSE	root mean square error
SD	standard deviation
T	dynamometer loading
u	velocity vector
v	circumferential velocity

Subscripts

in	inlet
max	maximum
out	outlet
tot	stagnation

Greek letters

α	angle of the draft tube
ρ	density
ϕ	flow coefficient

and the new design showed a peak efficiency of 95.3% for the optimized case, which was 3.3% higher than the original turbine efficiency. That efficiency peak was obtained at an approximate turbine power of 100 MW, about 23% higher than the existing runner power at the rated condition.

Madsen and Langthjem [6] optimized the wall shape of a two-dimensional incompressible diffuser to obtain its maximum pressure recovery factor (PRF). They used the response surface technique to estimate the objective function; and their derivative-based optimizer achieved a design with a higher area ratio (AR) than the ratio suggested in the literatures. They found that a convex-outward or bell-shaped design for the diffuser achieves a higher performance [7]; however, the response surface optimization produced a design which is mostly bell shaped with the end of the diffuser wall bent outward. The optimization results were the same for different CFD codes.

Marjavaara et al. [8] employed multiple surrogates in combination with the NSGA-II algorithm to optimize the shape of a simplified diffuser utilized in Francis turbines. They used five geometric design variables under two different operating conditions. Both the Response Surface (RS) methodology and Radial Basis Neural Network (RBNN) were considered to approximate the surrogate model. The analysis of the Pareto optimal solutions revealed that the fidelity of the RBNN is generally higher than the RS model. The predictive capabilities of the RBNN models were also better near the Pareto front; although the reliability of the quadratic models in this region was poor.

Shojaeefard et al. [9] showed that the swirl components of the inlet velocity vector are the most important performance parameters in the shape optimization of draft tubes. They found that the pressure recovery factor increases with the height and angle values over the design ranges.

The goal of present study is to optimize the shape of draft tube used in Agnew turbines. A surrogate-based optimization approach was implemented to redesign the shape of straight-divergent type of draft tube in an Agnew turbine. An artificial neural network (ANN) as a surrogate model is applied for optimization the design of draft tube and numerical simulations are performed to introduce the final design. The new design is then manufactured and installed at the outlet of the turbine in HML. The performance of the new draft tube is experimentally evaluated under various operating conditions.

2. System description

The schematic view of the turbine is presented in Fig. 1. As shown in the figure, Agnew turbine consists of four main parts: the casing, the runner and blade assembly, the housings, and the draft tube [2]. The turbine casing is flanged to the pipeline of the test rig, which has been designed in a way that changes the flow direction from horizontal to the direction of turbine's rotation axis. The turbine installed at the HML of the IROST has four rotating blades of 75 mm tip radius and 2.5 mm radial tip clearance. The housings consist of two bearings and sealing assembly. All the bearings are placed in the housings to restrain the radial and axial movements of the shaft. The sealing prevents water from leaking into the bearings. The draft tube is a simple straight pipe connected to the inlet of the casing. By reducing the kinetic energy loss at the outlet, the draft tube produces a negative head at the runner exit and improves the efficiency.

The design variables in the shape optimization problem of the draft tube are its height above the tailrace (H), and the cone angle (2α). Based on the physical constraints of the test rig, the lower and upper bounds for the height of the draft tube are 250 mm and 1500 mm, respectively. Besides this, the cone angle should be limited to less than 8°, according to the literature [10]. As the flow moves downstream and forms vortices and circulatory eddies, it detaches away from the wall and causes higher head losses at larger angles. For optimization purposes, the upper bound of the cone

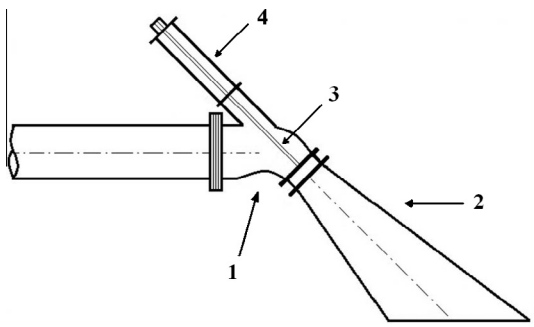

Fig. 1. Schematic view of Agnew turbine: (1) casing, (2) draft tube, (3) main shaft and (4) bearings housing.

angle was set to 10°, to take a wider design range into consideration.

The main goal of installing a draft tube in the reaction hydraulic turbines is to recover the wasted kinetic energy at the runner outlet. Kinetic energy increases in proportion to the specific speed of a turbine; and in the case of Kaplan turbines, it is nearly 45% of the net working head [10]. The performance of a draft tube is evaluated by the following expressions for the pressure recovery factor (PRF) and the energy loss coefficient (ELC):

$$\mathrm{PRF} = \frac{\frac{1}{A_{out}}\iint_{A_{out}} p dA - \frac{1}{A_{in}}\iint_{A_{in}} p dA}{\frac{1}{2}\rho\left(\frac{Q_{in}}{A_{in}}\right)^2} \tag{1}$$

$$\mathrm{ELC} = \frac{\iint_{A_{in}} p_{tot}\boldsymbol{u}.\boldsymbol{n} dA - \iint_{A_{out}} p_{tot}\boldsymbol{u}.\boldsymbol{n} dA}{\frac{1}{2}\rho\left(\frac{Q_{in}}{A_{in}}\right)^2} \tag{2}$$

For a simple one-dimensional modeling, it is suggested that [11]:

$$\mathrm{PRF} = 1 - \mathrm{ELC} - \frac{1}{\mathrm{AR}} \tag{3}$$

where AR is the ratio of the cross sectional area at the outlet to that at the inlet.

An optimization problem was defined to maximize the pressure recovery factor (PRF) of the draft tube of Agnew micro-hydro-turbine and to minimize its energy loss coefficient (ELC). This multi-objective optimization problem can be summarized as follows:

$$\text{Maximize} \quad F = (\mathrm{PRF}, 1 - \mathrm{ELC})^T \tag{4}$$

$$\text{Subject to}: \begin{cases} 0 < \alpha < 5 \\ \text{and} \\ 250 \leqslant H \leqslant 1500 \end{cases}$$

The design space has been specified in the above equation. The fidelity of the surrogate model is highly dependent on the number and distribution of the design points throughout the design space. The Design of Experiment (DOE) strategy was adopted to select a set of design points. The method of Face-Centered Composite Design (FCCD) was applied to distribute 80 design points.

3. Experimental approach

3.1. Test rig and instrumentation

The open-circuit test rig for examining the performance of the Agnew turbine has been schematically illustrated in Fig. 2. This test rig consists of four main components: a 20 m^3 reservoir containing the water required for the test. Six pumps, each connected to an 11-kW electromotor, are arranged in parallel to provide the desired heads and flow rates. A long pipeline has been selected to ensure fully developed flow conditions at the turbine entrance. Also, a gate valve with a major head loss has been considered to get the required heads and flow rates.

3.1.1. Instrumentation

During the testing procedure, five parameters are measured to determine the turbine behavior at an operating point: the torque applied on the main shaft and its rotational speed, the flow rate, and the pressures at the turbine upstream and draft tube inlet. These pressure values are used to determine the effective turbine head and the suction head of the draft tube, respectively.

Flow rate. Since the transient-time flowmeters are non-intuitive, can be monitored, and have a reasonable price, a clamp-on type of this meter is used to determine the flow rate of water through the piping. The linear precision of this flow meter is 0.5% and its overall accuracy ranges from 1% to 3%. The clamp-on transducers are installed in the reflect-mode configuration. For each run, it takes a few minutes to establish the average values of the aforementioned parameters and to minimize the precision error.

Pressure. To determine the water head, pressure is measured at the turbine upstream and the inlet of the draft tube. The effective turbine head is determined by the pressure at the turbine upstream, while the suction head of the draft tube is ascertained by the pressure at the inlet. The first pressure tap is located far enough from the turbine upstream, and the second tap is located at the draft tube inlet. They are installed normal to the wall on the vertical side to avoid air and dirt in filtration. The pressure at the turbine upstream is measured by a piezoelectric transducer with a total precision of 0.13% over the whole operating range from 0.0 to 2.0 bars. The suction pressure of the draft tube is measured by a differential pressure gauge with a calibrated precision of 0.5%. The atmospheric pressure data was obtained from the nearest weather station located 10*km* from the lab.

Torque. In the research conducted by Yassi and Hashemloo [2], the torque generated by water flow passing across the runner was measured by an eddy current dynamometer, which has unfavorable levels of control stability and control response and needs cooling, especially under high-load operations. The new dynamometer used at the HML has a DC motor, and the mentioned problems are rectified. The accuracy of the load cell measuring the brake power on the shaft is ±1%.

Rotation speed. An electromagnetic induction type tachometer measures the rotational speed of the main shaft with an overall accuracy of ±0.1%. The teethed disk, which is linked to the shaft, rotates in the magnetic field induced by the tachometer and produces a sinusoidal signal by which the speed can be determined.

3.1.2. Measurement system

A series of tests are carried out to investigate the performance of the turbine components under various operating conditions. According to ASME PTC 18 [12] and IEC 60193 [13], the test data are sampled during both the rise and fall of dynamometer load when the runner spins at a specific rotational speed. Each test procedure is carried out three times to be sure of the repeatability of the results. The rotational speed of the runner is controlled by the dynamometer, while a number of pumps and valves regulate the flow conditions, including the flow rate and head at the turbine upstream. However, in this study, valves are not used to control the head. All the measuring devices are calibrated before the tests to remove the deviations and minimize the bias error [14].

4. Optimization approach

The surrogate-based optimization is an economical and reliable method for solving the optimization problems [15]. The surrogate model can also provide an insight into the functional relationship between design variables and optimization goals. The most famous approaches in this regard are the response surface models [16,17], neural networks [18], and the kriging [19,20] and radial basis approximations [21]. These approaches have been compared in the literature [22,23] and it has been shown that the selection of

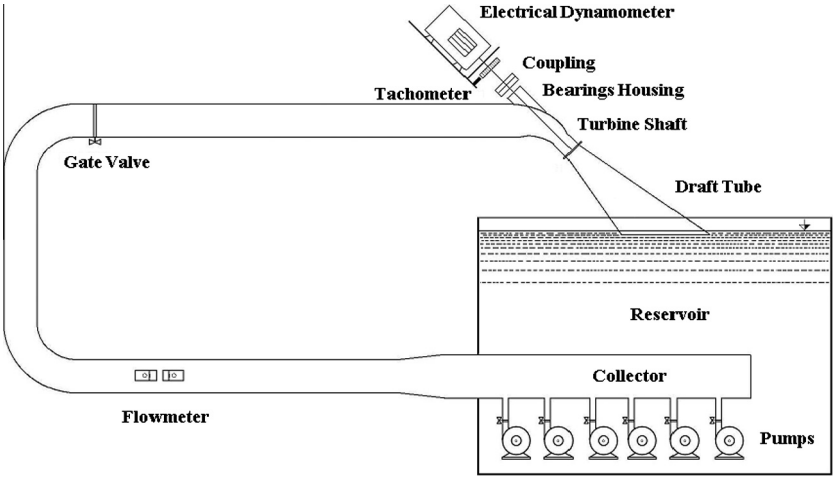

Fig. 2. Schematic of the test rig at the HML.

the best approach is dependent upon the specific problem involved.

In this study, an Artificial Neural Network (ANN) approach was adopted as the surrogate model together with the non-gradient based optimization algorithm of NSGA-II developed by Deb [24] to design the shape of the draft tube for an Agnew micro-hydro-turbine. This procedure is explained step-by-step in the following section.

4.1. Numerical simulations

All the numerical simulations have been carried out by means of the open-source code "OpenFOAM", which is a Finite Volume Method (FVM) solver and which uses the "SIMPLE" algorithm to correlate the coupling of pressure and velocity [25]. In order to discretize the convective terms, the "QUICK" method was implemented, while the second order accuracy of the central differencing scheme was applied to discretize the viscous terms.

The turbulence in the fluid flow was modeled by the Shear Stress Transport (SST) model to exploit the advantages of the k–ε model in solving the far-wall regions and those of the k–ω model for the near-wall treatment. The wall-function was used to model the flow near the wall. The geometry discretization was carried out by the H-grid topology, as the maximum value of Y^+ over the draft tube wall was below 100.

All the solutions were judged to be convergent when the residuals were under 10^{-5}. Moreover, the flow rate and pressure at the inlet were controlled to stay steady when the solutions were interrupted.

4.1.1. Boundary conditions

According to Table 1, the measured values of flow rate for different numbers of working pumps were considered as the inlet boundary condition (BC), while the atmospheric pressure was taken as the outlet BC. At the inlet, the flow swirl and the intensity of the incoming flow should be determined. The inlet swirl is dependent on the rotational speed of the turbine runner and its values are determined from the measurements of torque and rotational speed for the runner and by using the Euler's work equation [26].

The intensity of the flow at the downstream of turbine runner is unknown. It can be predicted by gradually changing its value and comparing the simulation and experimental results. However, the turbulent intensity of the inlet flow has a lesser effect on the performance of hydraulic machine components than it does on the compressible flow of turbomachines, like the combustion chambers in gas turbines. As recommended by Denton [27], the CFD results per different values of flow intensity were used to calibrate the inlet turbulence. The difference between the objective functions was not noticeable for the values of $I = 2\%$, 3.5% and 5%; however, $I = 3.5\%$ was the value best matched with the experimental data.

Table 1
Boundary conditions for different numbers of working pumps.

No. of working pumps	Average flow rate (L/s)	Flow ratio (Q/Q_{max})	PRF	ELC
2 Pumps	39	0.557	0.671	0.201
3 Pumps	49	0.700	0.653	0.218
4 Pumps	65	0.928	0.660	0.210

4.2. Model construction

The values of the pressure recovery factor (PRF) and the energy loss coefficient (ELC) calculated from the numerical simulations were used to build the surrogate model. To this end, a feed-forward neural network was selected to assess the global behavior of each objective function. From among the design points, 62 data were selected to train the surrogate neural networks, while the remaining 18 design data were used to test the predictive capability of the network. In order to achieve the best fitted networks, a number of neurons in the hidden layers, and in the weight, bias and activation functions were examined [9]. Finally, 25 neurons per layer, and the tan-sigmoid and linear activation functions for the hidden and output layers were selected to train the networks. Similar to the other surrogate models, the predictions of the built networks are associated with the errors including the bias and variance, which are determined by the Root Mean Square Error (RMSE) [28]. With respect to the pressure recovery factor, the RMSE values for network training and network validation were 1.41% and 1.32%, respectively; while these values were 1.27% and 0.85% with respect to the energy loss coefficient. More detailed discussion about construction and validation of the surrogate models of the PRF and the ELC has been presented in [9]. Fig. 3 presents the results of the objective function obtained from the numerical simulation versus those of the surrogate model for the training data and the testing data.

4.3. Optimal solutions

In the problem of shape optimization of the draft tube for Agnew turbines, the aims are to gain maximum pressure recovery

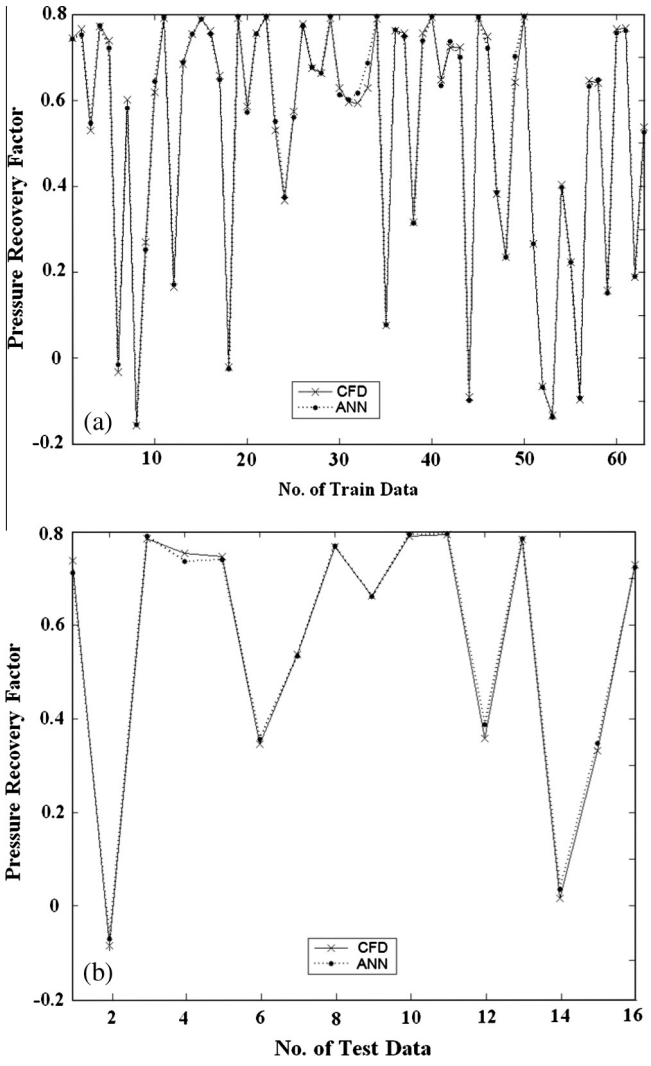

Fig. 3. The results of the CFD and ANN for (a) training and (b) testing cases and 4 working pumps.

factor and minimum energy loss. Although, the former can be achieved by selecting longer draft tubes and cone angles, but by doing so, the loss coefficient will increase and the turbine efficiency will diminish as a result. To establish a compromise between these conflicting objectives, a multi-objective optimization problem was defined. After training and validating the constructed neural networks, the obtained surrogate models of the pressure recovery factor and energy loss coefficient can now be incorporated to achieve the optimal designs. Genetic algorithms (GAs) are non-gradient-based methods, in which the solution convergence is less likely to occur in a local maximum, as the new generation is subjected to crossover and mutation operators. The modified version of the Non-dominated Sorting Genetic Algorithm, NSGA-II, developed by Deb et al. [29], was applied as the optimizer to explore any possible optimal solutions. Here a brief review of the principles is presented and the reader is referred to the literature for more detailed discussions [24,29]. Each generation, including the whole population of parents and offspring produced by the genetic operator, are sorted according to the non-dominance criteria. Since the size of the new population has doubled, the dominated population is eliminated based on a descending order of the crowding distance for the points located in the same fronts. The elite archive is updated by the new elite individuals, while the non-elitist solutions are discarded. This procedure is repeated for the maximum number of iteration, until all the non-dominated solutions are sorted into a set in the objective space, which is called the Pareto front [30].

In this study, the size of the population was set to 200, with the crossover and mutation rates being 0.8 and 0.4, respectively. The iterative procedure is terminated when 200 generations are analyzed.

One advantage of using the genetic algorithm as the optimizer is that a set of optimal solutions is achieved instead of a single optimum answer. Fig. 4a shows the Pareto optimal solutions to the multi-objective draft tube optimization problem, for different values of flow rates. Designs with shorter tubes yield lower loss coefficient values. Whereas those with longer tubes result in higher values of the pressure recovery factor (PRF). As is illustrated in Fig. 4b, the favorable designs are accomplished with the cone angle being in the range of 1.7–2.8° and the height being in the range of 550–1200 mm. The region of the longest designs yielding high PRF and the region of the shortest designs resulting in only low ELC are not taken into account to obtain favorable designs.

Limiting the design set of optimal solutions to contain a minimum PRF of 0.5 refines the Pareto fronts; while the lowest height to satisfy this constraint is 800 mm. Hence, three design points are selected from this region to be investigated in more details, see Table 2. The PRF and ELC values predicted by the ANN in the

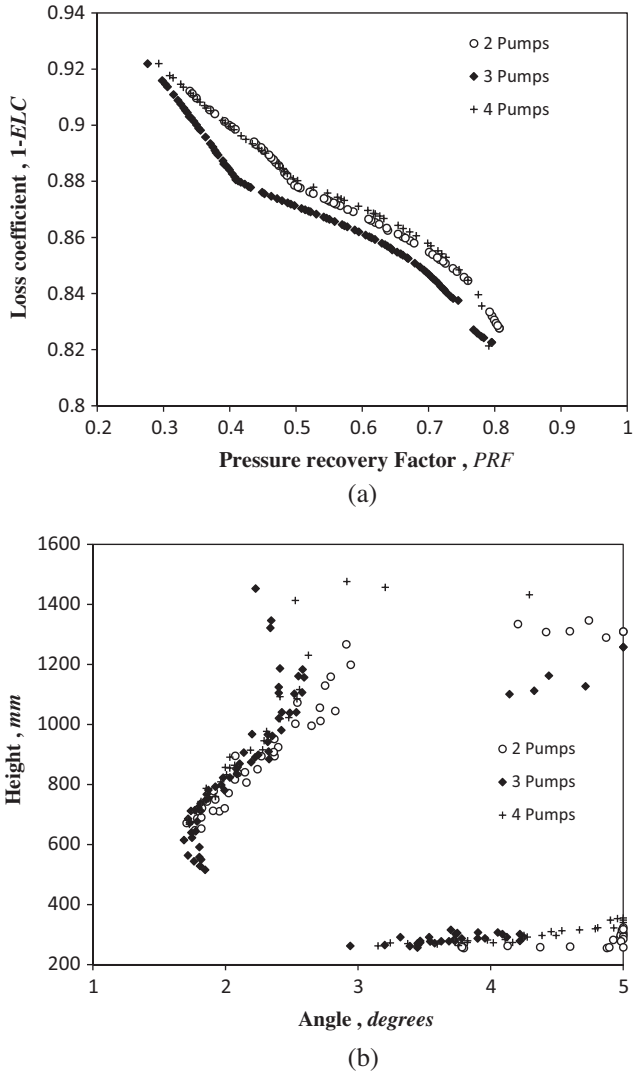

Fig. 4. Comparison of (a) Pareto optimal solutions and (b) the corresponding design data for different numbers of working pumps.

Table 2
The selected design data from the Pareto front.

Design	Q/Q_{max}	Geometry		CFD		ANN		Disparity (%)	
		α	H	PRF	ELC	PRF	ELC	PRF	ELC
A	0.577	1.82	721.6	0.523	0.131	0.542	0.126	6.61	−3.66
B	0.70	2.32	909.9	0.652	0.143	0.653	0.145	0.12	1.73
C	0.92	2.58	1116.2	0.718	0.152	0.726	0.147	1.16	3.21

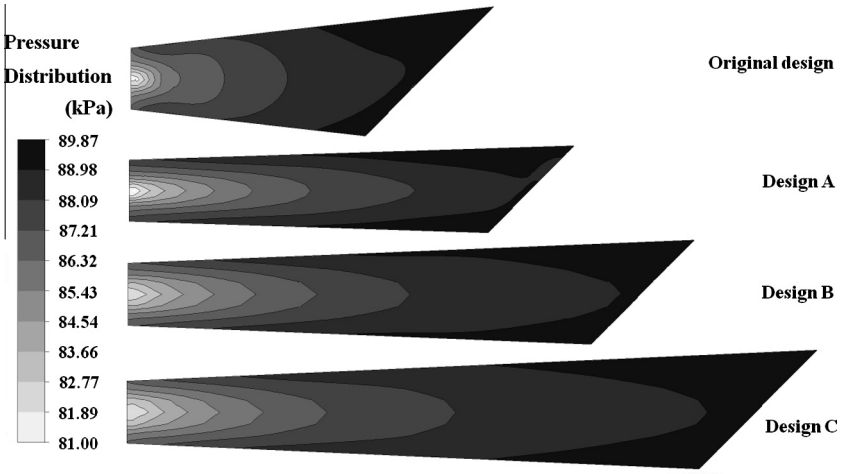

Fig. 5. Pressure contours for the selected optimal designs and the original design.

selected designs are compared against the outcomes of the numerical simulations. The pressure and velocity contours for three working pumps are also compared with those of the original design in Figs. 5 and 6, respectively. The low velocity region in the original design shown in Fig. 6, affects the performance of the draft tube. Given the low pressure recovery factor in Design A, it cannot be considered a proper choice. Having a reasonable size and a relatively high-pressure recovery factor, Design B is the most feasible design. Fig. 7a compares the manufactured Design B with the original design, while the installed draft tube at the turbine outlet is depicted in Fig. 7b.

As was discussed in Section 3, a series of tests are then carried out to investigate the behavior of the optimized model in practice. To control the operation of the turbine, the dynamometer induces a resistant torque on the main shaft, which reduces its rotational speed. According to the regulations, data should be taken in the increasing and decreasing modes of the dynamometer, which are shown in Fig. 8 by indexes "T" and "R", respectively. As the loading increases, the rotational speed of the runner diminishes; therefore, the circumferential blade speed ratio, k_u, decreases and so does the flow coefficient, $\phi = c_x/u$. The small difference between the loading and unloading curves is related to the losses of dynamometer in the "T" and "R" modes of operation.

In Fig. 9, the pressure recovery factor (PRF) of the original draft tube versus the blade speed and flow coefficient is compared for different operating conditions. As the loading increases, the swirl component of the velocity vector at the outlet grows rapidly, causing a drop in the draft tube performance. The higher the number of turned-on pumps, the higher the rate of flow that passes through the turbine and the larger the velocity triangles at the entry and exit of the runner. According to Eq. (1), the PRF becomes smaller when the inlet velocity increases with flow rate.

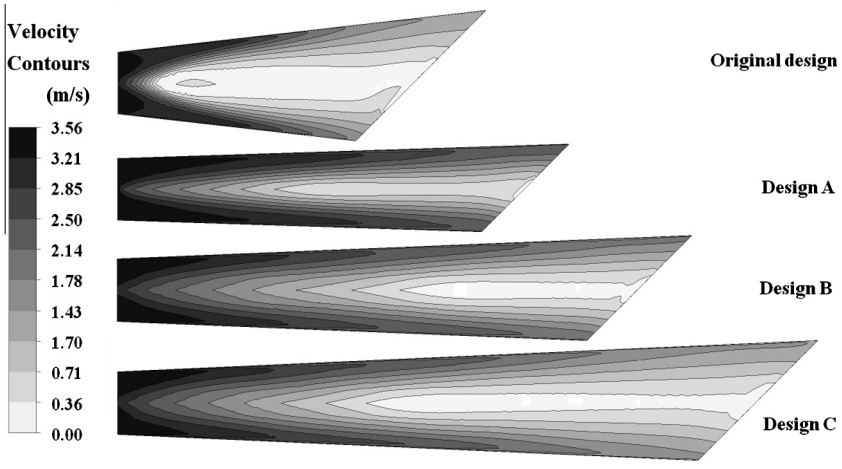

Fig. 6. Velocity contours for the selected optimal designs and the original design.

(a) (b)

Fig. 7. (a) The manufactured draft tube of Design "B" compared with the original design and (b) installed at the outlet of the Agnew turbine.

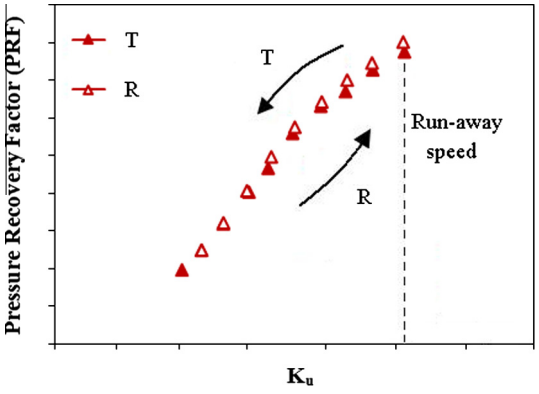

Fig. 8. Direction of turbine loading by the dynamometer in a typical performance chart.

Fig. 10 depicts the changes of the energy loss coefficient (ELC) for the original design in the entire operating range of turbine. The whirling flow wastes axial momentum and causes additional losses besides the energy dissipation through wall friction. For higher flow rates, the ELC is generally greater. As the dynamometer load increase, the swirl component of the velocity vector is amplified, causing more waste of energy and resulting in a greater loss coefficient.

The next figures present the results of the experiments conducted with the optimized draft tube and compare its performance to that of the original design. Since the modified draft tube is longer, the water depth in the reservoir is less in this case. The pumps suck the water from the tank and add approximately the same head to the fluid flow in both cases; hence, at the same flow rate, the fluid head at the upstream of turbine is less in the case of the modified draft tube. In the sequence of these variations in this case, the runner spins with lower rotational speeds in a run-away state. The run-away speed is the maximum attainable speed under maximum head when the external load, i.e. electrical force by the dynamometer, is disconnected from the turbine [31]. Therefore, the runner has a lower run-away rotational speed when the turbine is flanged to the modified draft tube.

Figs. 11 and 12 compare the PRF and the ELC values of the original draft tube (shown by "O") and the optimum design (denoted by "M") in the operation with the lowest flow rate. The curves show a similar trend, and we can see that the performance of the

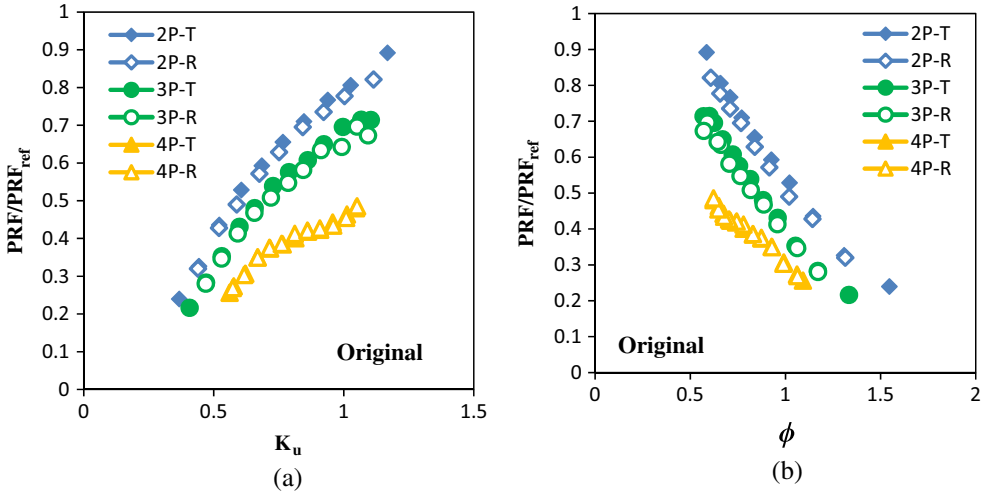

Fig. 9. The Pressure Recovery Factor (PRF) of the original draft tube versus (a) non-dimensional circumferential blade speed and (b) flow coefficient.

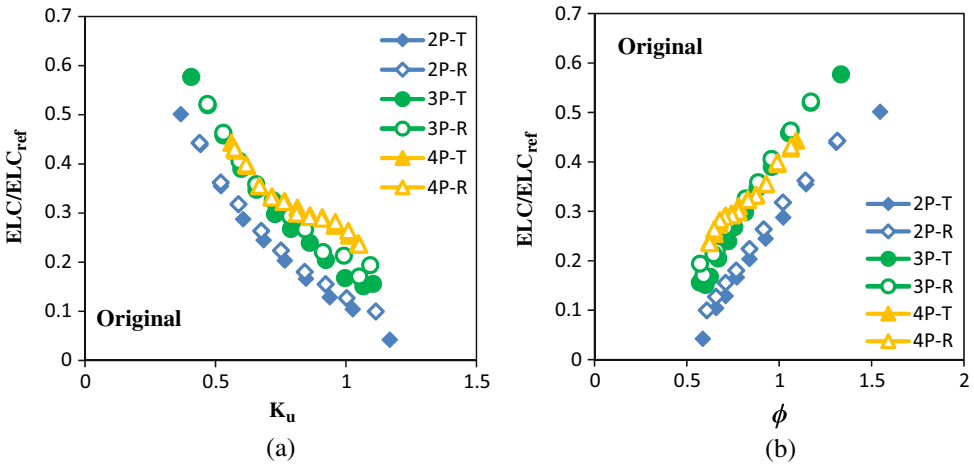

Fig. 10. The energy loss coefficient of the original draft tube (ELC) versus (a) non-dimensional circumferential blade speed and (b) flow coefficient.

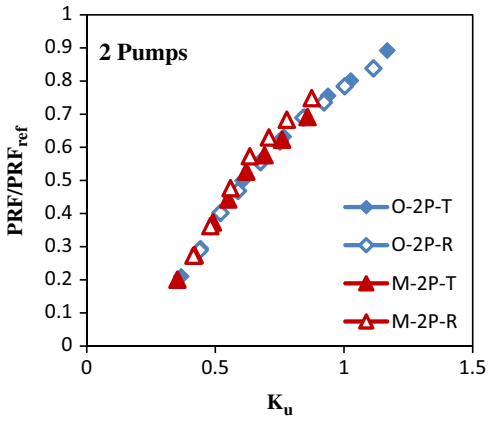

Fig. 11. Pressure recovery factors for two working pumps in the original and modified draft tube designs.

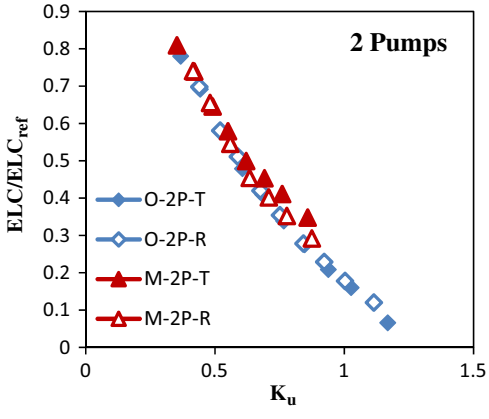

Fig. 12. Energy loss coefficients for two working pumps in the original and modified draft tube designs.

draft tube is greatly influenced by the runner speed and the swirl component of the incoming fluid flow. Since the water head at the upstream of turbine is not much different for the two cases, the curve of the optimized draft tube starts from a lower k_u value, due to a lower run-away speed. At higher loadings, the flow detaches from the wall, and the site observations indicate a poor draft tube performance at the lowest flow rate.

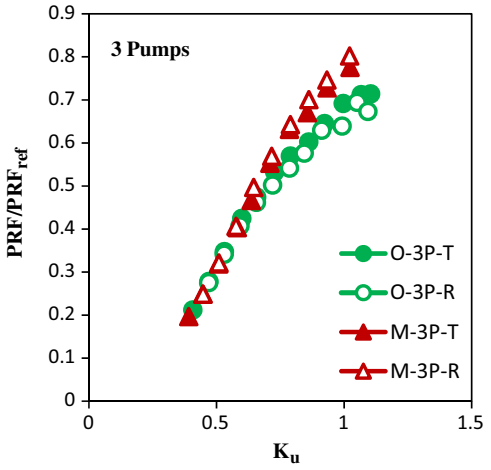

Fig. 13. Pressure recovery factors for three working pumps in the original and modified draft tube designs.

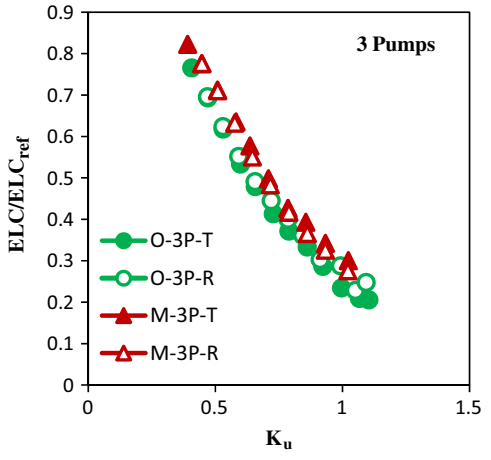

Fig. 14. Energy loss coefficients for three working pumps in the original and modified draft tube designs.

Figs. 13 and 14 depict the changes of performance variables PRF and ELC in the original and modified draft tube designs. The PRF and the ELC values in this case point out a successful modification

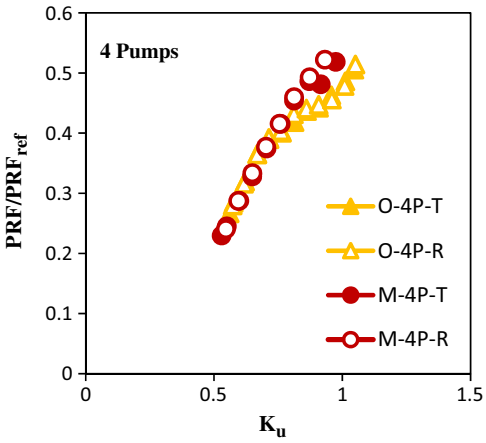

Fig. 15. Pressure recovery factors for four working pumps in the original and modified draft tube designs.

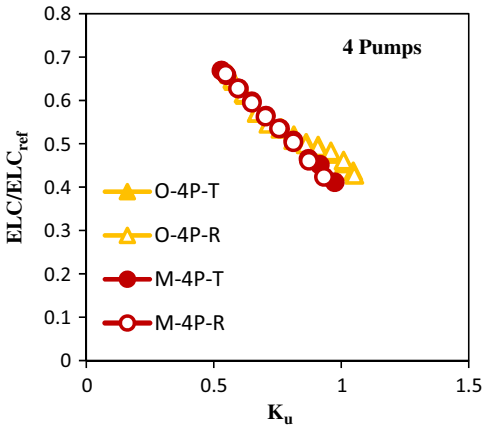

Fig. 16. Energy loss coefficients for four working pumps in the original and modified draft tube designs.

of the draft tube shape. The loss coefficient curves are identical, except for the low-loading region, where the fluid flow leaves the runner axially. With the increase in dynamometer brake load on the shaft, the flow vortex becomes stronger and affects the performance of the longer draft tube. The highest improvement in the PRF is achieved in the runaway speed when the swirl velocity is minimum. The non-dimensionalized PRF of the modified case is 20.3% higher in comparison with the original case for the runaway speed. The ELC is slightly increased due to the higher length of the draft tube in the modified case.

Figs. 15 and 16 illustrate the changes of the PRF and ELC values in the turbine's operating range when four pumps are working. A similar trend as in Figs. 13 and 14 is seen, but the difference between the two curves has become smaller. This is due to a higher flow velocity at the inlet of the draft tube, which yields lower values for the PRF and the ELC, according to Eqs. (1) and (2). The drop of the curve of the original draft tube in the high rotational velocities is removed for the modified case. The ELC is also reduced 4.0% with regard to its runaway value of the original draft tube. The PRF is also increased by 3.3% in the runaway speed.

Uncertainty of the measurements with the original and modified draft tube is determined in Tables 3 and 4. For each rotational speed, uncertainty is investigated from two aspects: Root Mean Square Error (RMSE) and Standard Deviation (SD). Both are listed in Table 3 for the PRF and ELC in the range of non-dimensional rotation speeds for the original turbine in two mode of the dynamometer; increasing and decreasing load. Experimental data is presented by the mean values, while the SD is considered as the confidence interval. The same terms for the modified turbine are presented in Table 4.

Table 3
Standard deviation (SD) and root mean square error (RMSE) of the PRF and the ELC for the original draft tube operating with three working pumps.

Unit speed ($N/\sqrt{H}$)	PRF		ELC	
	SD	RMSE	SD	RMSE
888.4	0.0084	0.0081	0.0089	0.0086
858.5	0.0028	0.0027	0.0030	0.0029
801.9	0.0072	0.0069	0.0077	0.0075
742.9	0.0088	0.0085	0.0096	0.0093
693.1	0.0053	0.0051	0.0057	0.0055
635.1	0.0031	0.0030	0.0032	0.0031
585.7	0.0022	0.0021	0.0025	0.0024
528.7	0.0025	0.0025	0.0030	0.0029
481.8	0.0020	0.0019	0.0023	0.0022
426.9	0.0041	0.0039	0.0045	0.0043
378.3	0.0020	0.0019	0.0023	0.0022
327.4	0.0024	0.0022	0.0027	0.0025
377.4	0.0020	0.0020	0.0023	0.0023
426.3	0.0023	0.0022	0.0026	0.0025
476.2	0.0018	0.0017	0.0020	0.0019
527.9	0.0021	0.0021	0.0025	0.0024
579.1	0.0050	0.0049	0.0055	0.0053
632.3	0.0023	0.0022	0.0026	0.0024
678.9	0.0014	0.0014	0.0016	0.0016
733.9	0.0048	0.0047	0.0053	0.0052
798.4	0.0034	0.0033	0.0037	0.0036
845.6	0.0071	0.0069	0.0077	0.0075
879.7	0.0033	0.0032	0.0036	0.0035

Table 4
Standard deviation (SD) and root mean square error (RMSE) of the PRF and the ELC for the modified draft tube operating with three working pumps.

Unit speed ($N/\sqrt{H}$)	PRF		ELC	
	SD	RMSE	SD	RMSE
823.4	0.0043	0.0041	0.0026	0.0025
751.1	0.0086	0.0083	0.0055	0.0053
688.8	0.0046	0.0045	0.0033	0.0032
632.3	0.0034	0.0034	0.0024	0.0023
570.5	0.0058	0.0057	0.0043	0.0042
511.8	0.0034	0.0033	0.0027	0.0026
467.8	0.0044	0.0043	0.0034	0.0033
409.1	0.0046	0.0045	0.0037	0.0036
359.1	0.0052	0.0051	0.0043	0.0042
314.6	0.0044	0.0043	0.0037	0.0036
359.7	0.0036	0.0035	0.0029	0.0028
409.8	0.0040	0.0039	0.0032	0.0031
463.7	0.0037	0.0036	0.0028	0.0028
519.5	0.0076	0.0074	0.0058	0.0057
576.4	0.0043	0.0042	0.0032	0.0031
635.3	0.0054	0.0053	0.0040	0.0039
693.6	0.0082	0.0081	0.0056	0.0056
750.5	0.0059	0.0058	0.0037	0.0037
822.1	0.0064	0.0063	0.0041	0.0041

5. Conclusion

In this work, the performance improvement of Agnew turbine components was studied. To improve the draft tube, a surrogate-based optimization approach was applied. Three probable choices from the optimal solutions were numerically investigated and Design B with $H = 909.9$ mm and $\alpha = 2.32$ was finally selected and manufactured. The new draft tube was installed at the outlet of an Agnew turbine studied at the HML. A Series of tests were then performed according to ASME PTC 18.0 and IEC 60193 to examine

the performance of the improved turbine in practice. The experiments were performed under different operating conditions with varying dynamometer loadings and different flow rates. The obtained results indicate that, except for the lowest flow rate ($Q/Q_{max} = 0.58$), the performance of the draft tube and, consequently, the turbine efficiency improve. At the lowest flow rates, the performance curves have a similar trend and the differences are negligible. The most significant improvement was achieved for the runaway speed at $Q/Q_{max} = 0.70$, where the PRF and the ELC values are arisen by 20.3% and 4.2%, respectively. At the highest flow rate ($Q/Q_{max} = 0.92$), the measurements are indicated an improvement of 3.3% in the PRF and a reduction of 4.0% in the ELC. The drop in the curves of the original draft tube is also removed. These results show a successful shape optimization for the components of the Agnew micro-hydro-turbine.

Acknowledgments

The authors wish to thank the personnel of the IROST for their help during the testing of the turbines. A special appreciation goes to Saeed Sharif Razavian for his valuable help with the preparation of the measuring devices. We also thank Jahanfar Zarghami, for his useful comments on the overhaul of the turbine, and Hamid Bakhtiari, Mohammad Bayrami, Amir Houshang Ghayyomi, Mohammad Ilanlou, and Karim Sadeghi for their support throughout this project. We also acknowledge Mr. Ali Dalirbod from R&D Department of MAPNA Group Co. for his useful comments.

References

[1] Yassi Y. An experimental study of improvement of a performance. Ph.D Thesis. Glasgow University: Glasgow, Scotland; 1999.
[2] Yassi Y, Hashemloo S. Improvement of the efficiency of the Agnew microhydro turbine at part loads due to installing guide vanes mechanism. Energy Convers Manage 2010;51(10):1970–5.
[3] Papoutsis-Kiachagias EM, Kyriacou SA, Giannakoglou KC. The continuous adjoint method for the design of hydraulic turbomachines. Comput Methods Appl Mech Eng 2014;278:621–39.
[4] Lipej A. Optimization method for the design of axial hydraulic turbines. Proc Inst Mech Eng Part A: J. Power Energy 2004;218:43–50.
[5] Wu J, Shimmei K, Tani K, Niikura K, Sato J. CFD-based design optimization for hydro turbines. Trans ASME J Fluids Eng 2007;129(2):159–68.
[6] Madsen J, Langthjem M. Multifidelity response surface approximations for the optimum design of diffuser flows. Optimization Eng 2001;2:453–68.
[7] Madsen J, Shyy W, Raphael T. Response surface techniques for diffuser shape optimization. AIAA J 2000;38(9):1512–8.
[8] Marjavaara BD, Goel T, Shyy W, Mack Y, Lundström TS. Hydraulic turbine diffuser shape optimization by multiple surrogate model approximations of Pareto fronts. Trans ASME J Fluid Eng 2007;129(9):1228–40.
[9] Shojaeefard MH, Mirzaei A, Babaei A. Shape optimization of draft tubes for Agnew microhydro turbines. Energy Convers Manage 2014;79:681–9.
[10] Lal J. Hydraulic machines. 6th ed. Metropolitan Book Co.; 1995.
[11] Japikse D, Baines NC. Diffuser design technology, Concept ETI; 1998.
[12] ASME Perfromance Test Code 18.0. Hydraulic turbines. New York: ASME; 1992.
[13] International standard, IEC 60193. Hydraulic turbines, storage pumps and pump-turbines – Model acceptance tests. International Electrotechnical Commision; 1999.
[14] Fuller WA. Measurement error models. John Wiley & Sons; 1987.
[15] Queipo NV, Haftka RT, Shyy W, Goel T, Vaidyanathan R, Tucker PK. Surrogate-based analysis and optimization. Prog Aerospace Sci 2005;41:1–28.
[16] Betiku E, Taiwo AE. Modeling and optimization of bioethanol production from breadfruit starch hydrolyzate vis-a-vis response surface methodology and artificial neural network. Renew Energy 2015;74:87–94.
[17] Atmanli A, Yüksel B, İleri E, Karaoglan AD. Response surface methodology based optimization of diesel–n-butanol–cotton oil ternary blend ratios to improve engine performance and exhaust emission characteristics. Energy Convers Manage 2015;90:383–94.
[18] Azadeh A, Babazadeh R, Asadzadeh SM. Optimum estimation and forecasting of renewable energy consumption by artificial neural networks. Renew Sustain Energy Rev 2013;27:605–12.
[19] Simpson TW, Mauery TM, Korte JJ. Kriging models for global approximation in simulation-based multidisciplinary design optimization. AIAA J 2001;39 (12):2233–41.
[20] Li M, Li G, Azarm S. A kriging metamodel assisted multi-objective genetic algorithm for design optimization. Trans ASME J Mech Des 2008;130 (3):031401. 1–10.
[21] Fischer GR, Kipouros T, Savill AM. Multi-objective optimisation of horizontal axis wind turbine structure and energy production using aerofoil and blade properties as design variables. Renew Energy 2014;62:506–15.
[22] Jin R, Chen W, Simpson TW. Comparative studies of metamodelling techniques under multiple modelling criteria. Struct Multidisciplinary Optimization 2001;23(1):1–13.
[23] Goel T, Haftka RT, Shyy W, Queipo NV. Ensemble of surrogates. Struct Multidisciplinary Optimization 2007;33(3):199–216.
[24] Deb K. Multi-objective optimization using evolutionary algorithms. Chichester (London): John Wiley & Sons Inc; 2001.
[25] OpenFOAM. User guide; 2011.
[26] Yahya SM. Turbines, compressors and fans. 2nd ed. New Delhi (India): Tata McGraw-Hill Publishing Co.; 2002.
[27] Denton JD. Some limitations of turbomachinery CFD. In: Proceedings of ASME Turbo Expo 2010. Glasgow UK, Paper no. GT2010-22540, 2010.
[28] Zhang X. A statistical approach for sub-hourly solar radiation reconstruction. Renew Energy 2014;71:307–14.
[29] Deb K, Pratap A, Agarwal S, Meyarivan T. A fast and elitist multiobjective genetic algorithm: NSGA-II. IEEE Trans Evol Comput 2002;6(2):181–97.
[30] Borhanazad H, Mekhilef S, Ganapathy VG, Modiri-Delshad M, Mirtaheri A. Optimization of micro-grid system using MOPSO. Renew Energy 2014;71:295–306.
[31] Krivchenko GI. Hydraulic machines: turbines and pumps. Moscow: Mir publishers; 1986.